nature communications

Article

https://doi.org/10.1038/s41467-025-60781-7

Unveiling hidden particle-level defects in glasses

Received: 27 November 2024

Accepted: 2 June 2025

Published online: 17 June 2025

Check for updates

Yuan-Chao Hu [1] & Hajime Tanaka [2,3]

In crystals, defects are well-defined and crucial to their mechanical properties. In contrast, the structural disorder in glasses makes it challenging to directly identify defects at the particle level. However, low-frequency quasi-localised modes (QLMs) in glasses provide valuable insights, acting as mechanical defects associated with shear transformation zones and soft spots. Using molecular dynamics simulations of two-dimensional glasses, we identify a particle-level defect responsible for generating QLMs. The primary QLM originates from a "key-core" square of four particles vibrating in a two-in, two-out pattern, interpretable as a microscopic Eshelby inclusion. The motion of these particles induces nearby volumetric and far-field shear deformations, forming a characteristic four-leaf pattern. Despite the structural isotropy of the glass, these QLMs introduce notable mechanical anisotropy, particularly in nano-sized glasses. Crucially, pinning the key-core particles dramatically reduces shear modulus anisotropy, confirming their role as "localised particle-level defects." This discovery deepens our understanding of glass defects and offers valuable insights for nanoscale glass applications.

Identifying structural defects is crucial for advancing both scientific understanding and industrial applications of crystalline materials. In materials science, establishing a clear relationship between structure and properties has been a central focus, and this approach has proven effective for crystals. In crystalline materials, defects are identifiable from static atomic arrangements due to their well-defined positional order, with structural defects directly corresponding to mechanical defects.

However, the challenge intensifies when dealing with amorphous materials. The absence of long-range atomic order in these materials complicates the identification of defects. Unlike crystals, where defects are discernible from the well-defined structural framework, amorphous materials require alternative methods for defect characterisation. The lack of a regular atomic structure means that traditional definitions and approaches to defects, which work well for crystals, are not directly applicable to amorphous materials. This necessitates the development of novel techniques and concepts to understand and define defects in these disordered systems.

This complexity motivates a shift in perspective towards vibrational dynamics as a means to uncover and characterise defects in amorphous solids. In ideal crystals, vibration excitations are well-defined as the Goldstone modes (i.e. phonons) arising from the breakdown of continuous translational symmetry. This symmetry-breaking explains the sharp emergence of static shear elasticity upon crystallisation. However, when defects are present, crystals exhibit quasi-localised vibrational modes in addition to phonons. In such crystals, defects correlate with structural disorder, allowing straightforward identification.

Applying this understanding to glasses is challenging due to their intrinsic structural disorder. However, examining their vibrational features provides a valuable approach to exploring defects in these materials. Unlike crystals, glasses exhibit unique vibrational properties marked by nonphononic low-frequency modes, often termed quasi-localised modes (QLMs)[1,2]. These QLMs are thought to underlie the anomalous physical properties of glasses at low temperatures[3], such as the linear temperature dependence of the heat capacity $C(T)$—in

[1]Songshan Lake Materials Laboratory, Dongguan 523808, China. [2]Research Center for Advanced Science and Technology, The University of Tokyo, 4-6-1 Komaba, Meguro-ku Tokyo, Japan. [3]Department of Fundamental Engineering, Institute of Industrial Science, The University of Tokyo, 4-6-1 Komaba, Meguro-ku Tokyo, Japan. e-mail: yuanchao.hu@sslab.org.cn; tanaka@iis.u-tokyo.ac.jp

contrast to the T^3 scaling predicted by Debye for crystals—and the presence of a peak in $C(T)/T^3$ around 10 to 30 K, known as the boson peak[4–8]. Additionally, glasses show a T^2 dependence of thermal conductivity, deviating from the T^3 scaling associated with phonon-mediated heat conduction as per Debye's theory. Notably, the thermodynamic and transport anomalies observed below 1 K have been attributed to two-level tunnelling systems, which may be linked to QLMs[9,10].

Therefore, understanding the microscopic nature of QLMs is essential for comprehending the glassy state, particularly in the context of identifying the structural defects that govern dynamics—a longstanding challenge in glass physics[11,12]. Previous studies have investigated fundamental properties of QLMs, such as their long-range characteristics and their association with force dipoles[13–17]. More recently, QLMs have received renewed attention due to their connection to marginal stability and their influence on the thermal and mechanical properties of glasses and jammed systems (see ref. 2 for a review). From a mechanical perspective, concepts like shear transformation zones (STZs)[18,19] and soft spots[20] are particularly important. STZs and soft spots have been shown to predict the locations of particle rearrangements under deformation in various systems, including computer glass models[20], polymer glasses[21], colloidal glasses[22], metallic glasses[23,24] and even imperfect colloidal crystals[25].

Recently, it has also been proposed that the locations of plastic events under quasistatic shear strongly correlate with topological defects in the eigenvector fields that have a negative charge[26]. Such topological defects have recently been directly observed in a two-dimensional (2D) colloidal glass[27], where their density was found to correlate strongly with vibrational anomalies. In polymer glasses under shear, these defects were found to anti-correlate with non-affine displacement magnitude and to cluster near the yielding point[28], suggesting their mechanical significance extends across material classes. Complementing this view, Şopu et al. proposed a mechanism for shear banding in metallic glasses that emphasises the autocatalytic emergence of strong strain and vortex-like rotation fields[29,30]. These structures, corresponding to STZs, offer a mesoscale pathway from local defects to macroscopic flow. Their connection to QLMs—particularly in terms of collective excitation and energy dissipation—remains an important open question.

Soft spots, by definition, encompass low-frequency QLMs, phononic modes, and their hybridisations[20,22,25], representing their superimposed nature. Recognising this complexity, recent research has focused on disentangling QLMs from phononic modes and understanding their connection to soft spots[31–34]. QLMs have been identified as fundamental units for plastic instability[33], and are sometimes referred to as 'defects' or 'quadrupolar defects'[9,35]. Previous research has identified the cores of low-frequency QLMs, responsible for mechanical properties, as regions where the far-field power-law decay of vibrations begins[33,36]. These cores have conventionally been believed to have a relatively isotropic shape and consist of a few tens of particles in 2D systems. Consequently, these cores are considered fundamentally distinct from the more localised defects in crystals. However, the exact nature of glassy defects remains elusive, necessitating further investigation to fully understand their characteristics and their impact on the material properties of glasses.

While the role of quasi-localised modes (QLMs) in glass mechanics is increasingly recognised, the precise microscopic origin of these modes—and their classification as true defects—remains unresolved. Our work provides a definitive identification of a localised four-particle structure, the 'key-core square', that governs both the emergence and mechanical impact of primary QLMs.

In this study, we address these challenges by examining the particle-level structure and vibration modes using extensive molecular dynamics (MD) simulations of 2D model systems. In glasses, QLMs typically exhibit an unstable core surrounded by a stable far-field component. Contrary to the conventional understanding that the core structure of QLMs consists of a few tens of particles, our findings reveal that the key core size of primary QLMs remains consistently small, similar to point defects in crystals.

The key-core structure in a 2D system is typically composed of four particles arranged in a square configuration, vibrating in a two-in, two-out manner. It is often accompanied by strings of particles with high vibrability[37], which quantifies susceptibility to infinitesimal thermal excitation at zero temperature. The orientation of the resulting four-leaf pattern and the anisotropy in the shear modulus are primarily governed by the arrangement and orientation of these key-core squares and the associated particle strings. This suggests that primary QLMs originate from local defects that introduce mechanical frustration into the surrounding matrix. This enables us to redefine the conventional core of a QLM.

While the core has traditionally been defined by the onset of a long-range shear strain field with a power-law decay[33,36], we now reinterpret it as a region of disordered volumetric vibrations driven by the key-core square. In our 2D system, 'volumetric' specifically refers to local area fluctuations. Crucially, pinning these key-core squares nearly eliminates both the QLMs and the associated mechanical anisotropy, thus identifying them as localised mechanical defects in glasses. Strikingly, similar behaviour is observed in single-component crystals containing point defects[38].

The local nature of these defects is particularly evident in easily excitable low-frequency 'primary QLMs', which have a significant impact on mechanical properties. Additionally, we identify secondary defects that are more spatially extended, revealing a hierarchical organisation of defects—a distinctive feature of glasses with structural disorder. This hierarchical nature aligns with the power-law-like scaling of the vibrational density of states with angular frequency ω^2, a signature feature of QLMs.

These results provide novel insights into the vibrational and mechanical properties of glasses and crystals, introducing a new method for identifying defects at the particle level mechanically. Importantly, our findings have significant implications for nanoscience: even in structurally isotropic glasses, mechanical isotropy may not be preserved in small systems when defects are present. Therefore, careful avoidance or repair of defects, such as through annealing and mechanical training, is essential for optimising the performance of glasses and crystals in nanotechnology applications.

Results

We investigated the nature of mechanical defects in glasses using three distinct 2D model systems. The first two models are glasses: one uses an inverse power-law potential (2DIPL)[39,40], which is purely repulsive, and the other employs the classical Kob-Andersen potential (2DKA)[41], incorporating long-range attractions. Notably, the results from these models are consistent, with detailed findings from the 2DIPL model presented in the main text and those from the 2DKA model discussed in the Supplementary Information. The third model features a monatomic crystal with point defects, where interparticle interactions are described by the inverse power-law potential. Simulation details are provided in the Methods section.

Characterisation of low-frequency QLMs in glassy solids

We analyse the minimal-frequency vibration modes of the 2DIPL model by diagonalising its Hessian matrix at local minima of the energy landscape. In a large ensemble, most modes exhibit phonon-like characteristics, displaying high participation ratios (PR) and angular frequencies (ω) (see Supplementary Fig. 1). However, some modes show a continuous trend towards lower PR and ω, suggesting the presence of QLMs. This variation across samples raises intriguing questions about the underlying reasons for such differences.

To characterise the vibrational characteristics of QLMs, we decompose the vibrational modes into longitudinal and transverse

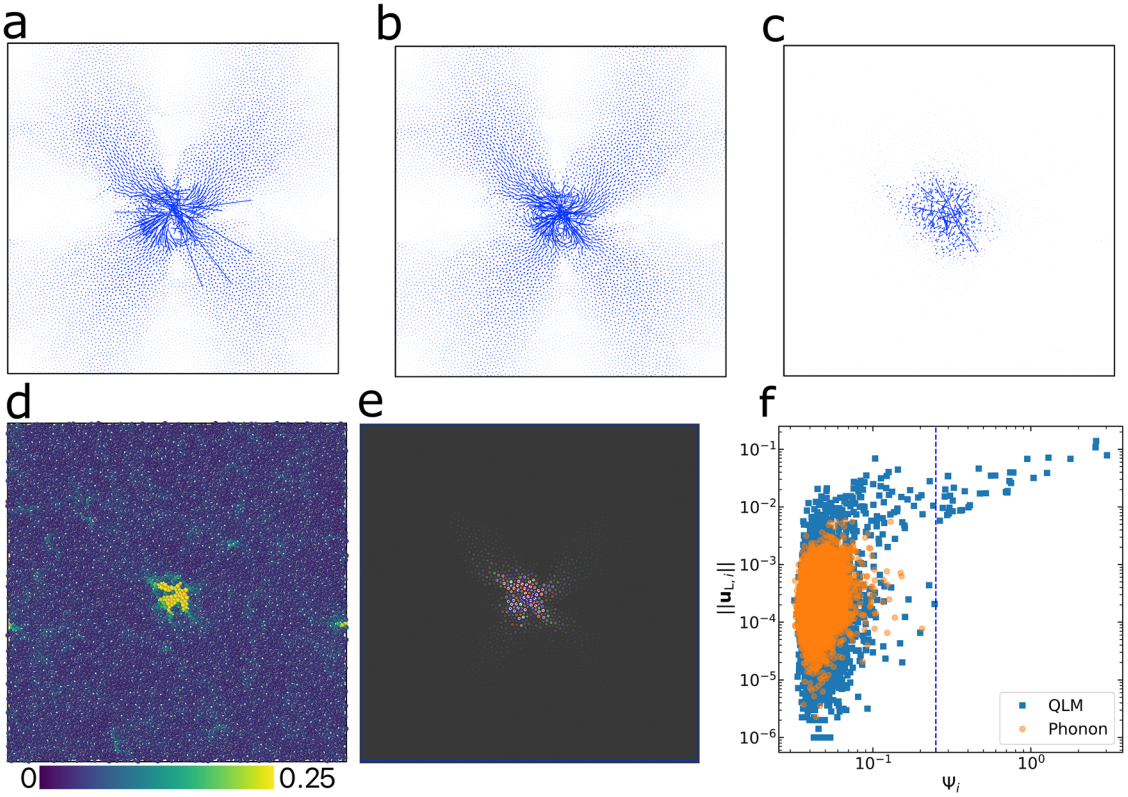

Fig. 1 | Real-space mode decomposition analyses of a typical QLM in 2DIPL. **a** Full eigenvector field of the QLM ($\omega = 0.164$, $PR = 0.005$). **b** Transverse component of the eigenvector field shown in (**a**). **c** Longitudinal component of the eigenvector field shown in (**a**). The magnitudes of the transverse and longitudinal components are 0.865 and 0.135, respectively. The core of the QLM is revealed by the longitudinal component in (**c**). **d** Vibrability Ψ field of the QLM, highlighting the core corresponding to (**c**). **e** The divergence ($\nabla \cdot \mathbf{u}_i^{\mathrm{np}}$) field of the net-projection vectors (arrows) of the eigenvector. Blue and red colours indicate regions of negative and positive divergence, respectively, while green represents areas with near-zero divergence. For clarity, only the central region of the QLM is shown, with particle transparency varying according to the magnitude of the vector. **f** Scatter plot of particle-level vibrability Ψ_i versus the magnitude of the longitudinal eigenvector $||\mathbf{u}_{L,i}||$. Data for a phonon mode is also included for comparison. The vertical dashed line indicates $\Psi_i > 0.25$.

components in real space using the Voronoi matrix method[40,42] (see Methods). In Fig. 1a–c, we illustrate the eigenvector field ($\mathbf{u}$) along with its transverse ($\mathbf{u}_{\mathrm{T}}$) and longitudinal ($\mathbf{u}_{\mathrm{L}}$) components for a QLM, clearly showing the characteristic four-leaf pattern. The core of QLMs displays randomness in both the direction and length of the vectors, highlighting a significant longitudinal component. This is particularly notable because ω is considerably lower than that of the first longitudinal phonon. Thus, the prominent longitudinal nature of vibrations in the core (Fig. 1c) is a distinctive feature of quadra-polar QLMs.

The cores of low-frequency QLMs have traditionally been identified as regions where the far-field power-law decay of vibrations begins[33,36]. Here, we characterise the cores of QLMs from a different perspective. To achieve this, we compute each particle's vibrability Ψ_i. Vibrability is defined as the susceptibility of particle motion to infinitesimal thermal excitation in the zero-temperature limit[37]:

$$\Psi_i \equiv \left.\frac{\partial\left\langle|\Delta\mathbf{r}_i|^2\right\rangle}{\partial T}\right|_{T=0} = \sum_{\lambda=1}^{2N-2}\frac{1}{\omega_\lambda^2}|\mathbf{u}_{\lambda,i}|^2, \tag{1}$$

with $\Delta\mathbf{r}_i = \mathbf{r}_i(T) - \mathbf{r}_i(0)$ denotes the displacement of particle i from its location at $T = 0$, and $<\cdot>$ represents the thermal average. The second equality holds under the harmonic approximation, with ω_l being the eigenfrequency of the l_{th} normal mode, and $\mathbf{u}_{l,i}$ the polarisation vector of particle i in this mode.

A higher value of Ψ_i signifies greater susceptibility to thermal excitation, indicating a more disordered or mechanically soft local environment[43]. Figure 1d shows the spatial distribution of Ψ_i, revealing a distinct core that aligns closely with regions exhibiting strong longitudinal vibrational components $||\mathbf{u}_{L,i}||$ in Fig. 1c. Notably, atoms with high Ψ_i also exhibit pronounced volumetric deformation, as reflected by elevated values of $\nabla \cdot \mathbf{u}_i^{\mathrm{np}}$ in the divergence field derived from the net-projection of the eigenvectors (Fig. 1e). This volumetric activity stems from the characteristic two-in, two-out vibrations of the key-core structure, which periodically induce the local atomic volume (area in 2D) changes in the surrounding particles (see Methods and Supplementary Fig. 2 for further details).

Although Ψ_i, $||\mathbf{u}_{L,i}||$, and $\nabla \cdot \mathbf{u}_i^{\mathrm{np}}$ are derived via distinct methodologies—thermal susceptibility, vibrational mode decomposition and vector field divergence, respectively—their spatial patterns display a notable and visually coherent overlap within the defect core. This convergence, clearly seen in Fig. 1c–e, underscores the robustness of the core's physical signature across multiple diagnostic lenses. Figure 1f further quantifies this relationship: particles with high Ψ_i generally exhibit stronger longitudinal displacements $||\mathbf{u}_{L,i}||$, particularly in the high-Ψ tail. This trend reinforces the use of Ψ_i as a sensitive and practical indicator for locating the QLM core, characterised by pronounced longitudinal motion. Supplementary Fig. 3 also provides a direct comparison between Ψ_i and $\nabla \cdot \mathbf{u}_i^{\mathrm{np}}$, revealing that particles with high Ψ_i frequently coincide with regions of pronounced, non-zero divergence. Notably, $\nabla \cdot \mathbf{u}_i^{\mathrm{np}}$ exhibits both positive and negative values with approximate symmetry, and its spatial distribution appears random—in stark contrast to the crystalline case (see below). This highlights the crucial role of structural disorder in shaping the core structure of QLMs. Furthermore, we confirm that regions with large vibrability ($\Psi > 0.25$) exhibit a near-zero net divergence on average,

indicating that, despite local volumetric fluctuations, the overall volume remains effectively conserved during mechanical deformation.

To assess these correlations more rigorously, we computed the Pearson coefficients between the relevant fields: (1) Ψ_i vs. $||\mathbf{u}_{L,i}||$: 0.66 (moderate positive correlation), (2) Ψ_i vs. $\nabla \cdot \mathbf{u}_i^{np}$: −0.085 (0.64 when using $|\nabla \cdot \mathbf{u}_i^{np}|$), (3) $||\mathbf{u}_{L,i}||$ vs. $\nabla \cdot \mathbf{u}_i^{np}$: -0.207 (0.68 with $|\nabla \cdot \mathbf{u}_i^{np}|$). The low correlation values involving $\nabla \cdot \mathbf{u}_i^{np}$ underscore that volumetric divergence is not linearly coupled to vibrability or longitudinal displacement −reflecting its nonlinear, possibly threshold-like nature. Nevertheless, the substantially higher correlations observed when using the absolute value of divergence confirm the strong visual alignment of high-intensity regions across the different fields. This convergence indicates that, while the descriptors capture different mechanical aspects, they consistently identify the same localised defect structures, reinforcing the physical coherence of the key-core region from multiple analytical perspectives.

Mechanical excitation of QLMs

To clarify the connection between QLMs and mechanical response[44–46,46,47], we applied minimal strain deformation to glass samples in an athermal quasistatic manner (see Methods). We then compared the resulting non-affine displacement fields with the eigenvector fields of the corresponding QLMs. In Fig. 2, we show two representative examples of QLMs, each exhibiting distinct spatial orientations.

First, we examine a 'regular' four-leaf pattern with an ~45° orientation (see Fig. 2a). We observe that a minimal strain perturbation through simple shear can effectively excite this QLM. The resulting

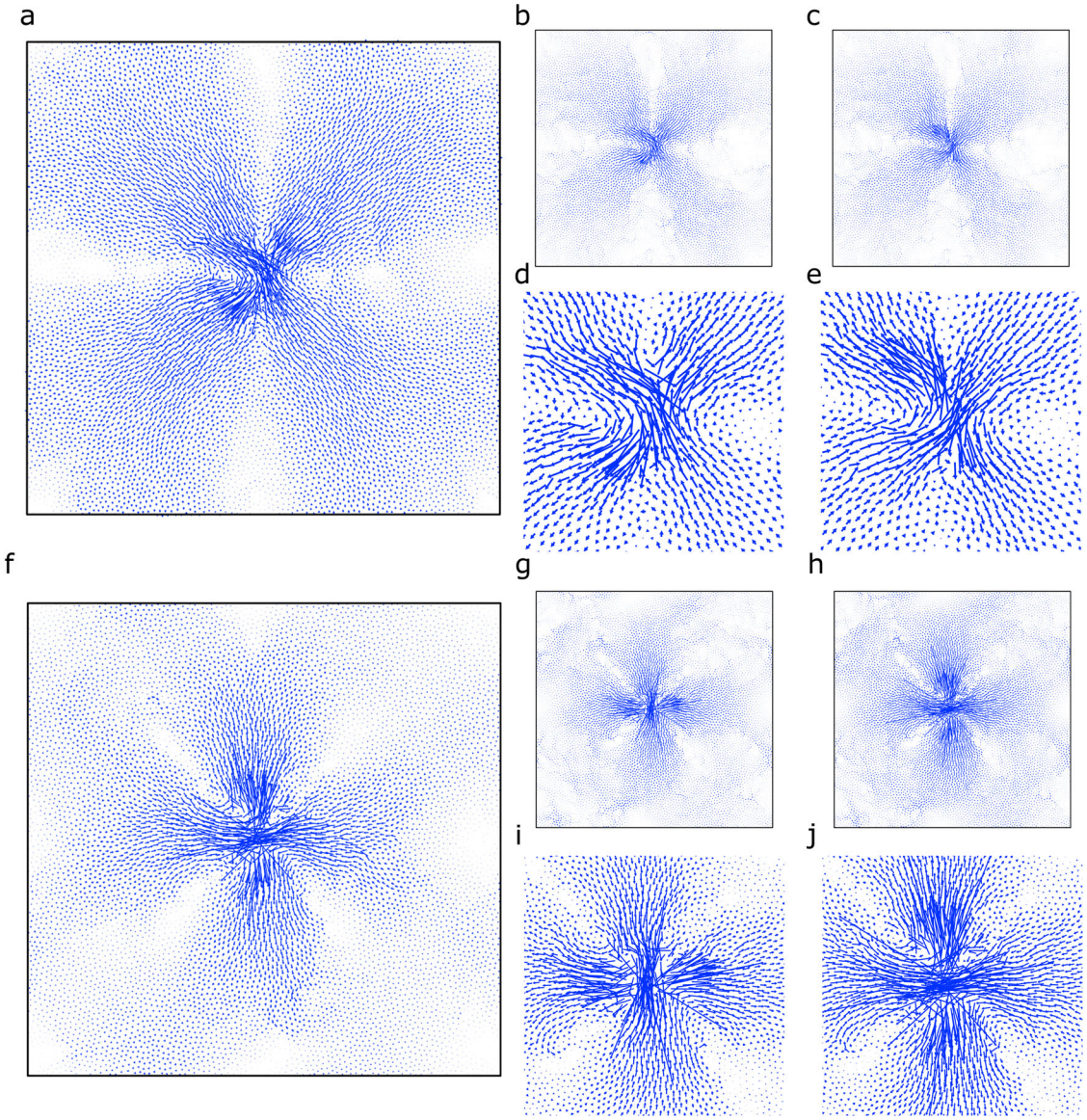

Fig. 2 | Excitation of QLMs through infinitesimal external strain. a–e Illustration of a glass sample with a QLM ($\omega = 0.154$, $PR = 0.050$) oriented close to 45°. **a** Eigenvector field of the QLM. **b** Non-affine displacement field under athermal quasistatic shear deformation along the positive direction of the horizontal axis. **d** provides an enlarged view of the central region from (**b**). **c** Non-affine displacement field under reversed shear direction. **e** provides an enlarged view of the central region from (**c**). Note that vector directions in (**d**, **e**) are opposite. Importantly, uniaxial tension and compression do not excite this QLM under similar conditions. **f–j** Illustration of another glass sample with a QLM ($\omega = 0.150$, $PR = 0.013$) oriented close to 90°. **f** Eigenvector field of the QLM. **g** Non-affine displacement field under athermal quasistatic tension along the horizontal axis. **i** provides an enlarged view of the central region from (**g**). **h** Non-affine displacement field under athermal quasistatic compression along the horizontal axis. **j** provides an enlarged view of the central region from (**h**). Note that the vector directions in (**i**, **j**) are opposite. We confirm that simple shear cannot excite this QLM under similar conditions.

non-affine displacement field closely mirrors the features of the eigenvector field, as shown in Fig. 2b, c. However, the direction of atomic displacement vectors varies depending on the deformation protocol. As highlighted in Fig. 2d, e, non-affine displacements emerge in opposite directions, with the magnitude of vectors differing in each case. This discrepancy likely arises from the orientation-dependent behaviour of shear moduli and the distinct characteristics of the key core structure. Notably, at this minimal strain level, neither tension nor compression effectively excites this QLM. The ~45° oriented QLM is particularly susceptible to shear deformation.

Next, we analyse a four-leaf pattern oriented at nearly 90° (see Fig. 2f). Interestingly, this QLM is easily activated by minimal tension or compression strains but remains unresponsive to simple shear at minimal strain levels. The non-affine displacement fields induced by tension (see Fig. 2g) and compression (see Fig. 2h) closely resemble the pattern observed in Fig. 2f. However, the directions of the displacement vectors in the two protocols are completely opposite, as shown in Fig. 2i, j. The ~90° oriented QLM is particularly susceptible to tension and compression.

Our investigation reveals a notable alignment between the net projection of eigenvectors from neighbouring atoms onto the central atom (see Methods) and the overall eigenvector field pattern. A detailed examination of the divergence field derived from these projections demonstrates that the cores of QLMs display non-zero divergence with approximately balanced positive and negative values, distributed in a seemingly random manner (see Supplementary Fig. 2). This finding supports the presence of disordered volumetric deformation within QLMs, reinforcing their intrinsically amorphous character.

If the four-leaf pattern is oriented between 0° and 90°, excluding 45°, all four deformation protocols can excite the QLM, though with differing intensities. The close spatial correspondence between the non-affine displacement field—arising from each protocol—and the eigenvector field of the QLM strongly supports its mechanical origin. These observations suggest that such QLMs function as dynamical defects, capable of dissipating energy under even minimal strain.

Interestingly, similar protocol-dependent responses have recently been observed in high-entropy alloys, where machine learning techniques were applied to unravel the complex correlations governing their deformation behaviour[48]. Inspired by this, future efforts could benefit from incorporating data-driven approaches—such as unsupervised learning or graph-based analysis—to systematically identify and classify key-core QLMs across a broader range of glassy systems. These approaches would not only complement physically grounded descriptors but also improve defect detectability in structurally complex or experimentally relevant systems.

These observations highlight the potential for subtle yet irreversible plastic deformation in glassy materials, even under minimal strain. Such deformation can arise while the system remains macroscopically within a nearly linear elastic regime, indicating that QLMs serve as the fundamental units of mechanical instability. These modes may be excited by infinitesimally small perturbations in an amorphous system near marginal stability, where no energy gap exists. This further underscores the inherently inelastic and anharmonic nature of amorphous solids[49–54].

Our findings support the view that QLMs originate from frustrated local force balances, a phenomenon intimately linked to the form of the interatomic potential. This aligns with recent work (e.g. ref. 55) showing that many-body interactions reduce local confinement, increasing susceptibility to infinitesimal excitations. These insights suggest a deep connection between the microscopic origin of QLMs and the underlying topology of the potential energy landscape, which varies across different interaction models. Investigating how the key-core defects identified in this study evolve under various potentials—especially those incorporating many-body terms—will be crucial for generalising the concept of QLMs across diverse material classes.

The direct correspondence between independent QLMs and non-affine displacement fields elucidates the intrinsic connection between QLMs and shear transformation zones (STZs) in glasses. This assertion is further supported by recent studies that identify QLMs using high-order expansions of potential energy[32,33]. From a mechanical perspective, distinct cubic modes exhibit four-leaf patterns and are correlated with plastic instabilities, such as local yielding[33,56]. The spatial orientation of these modes aligns with that of independent QLMs, reinforcing the idea that these four-leaf-type QLMs serve as the origin of soft spots[32]. Interestingly, cubic modes tend to converge towards QLMs devoid of phonons in the zero-frequency limit. However, the comprehensive isolation of QLMs from strongly hybridised phonons at higher frequencies through cubic modes remains to be confirmed in future research.

Identification of the key core structure of QLMs

Now, we delve into the critical question of what governs the core structure and orientation of these QLMs. One of our key discoveries are visually represented in Fig. 3 through two illustrative examples of glassy samples. First, we focus on atoms with substantial Ψ_i values (see Fig. 1f). These atoms form the fundamental core of a QLM, as depicted in Fig. 1d, and are further magnified in Fig. 3a1, b1 for two other glasses. This approach enables us to investigate the correlation between the number of particles in the QLM core, denoted as N_{core}, and its frequency, ω (refer to Fig. 3c). We observe that QLMs with larger cores tend to exhibit lower ω. However, establishing a precise quantitative relationship requires further investigation with more extensive datasets.

Interestingly, the core size of an isolated QLM, determined using this method, tends to saturate at approximately 20 atoms as the mode frequency ω increases. This value is consistent with the optimal atom count previously reported for soft spots in binary disordered packings with smaller system sizes[20].

Given that our simulation boxes are significantly larger than N_{core}, and the eigenvector fields associated with QLMs decay rapidly outside the defect core, we conclude that N_{core} is not subject to finite-size effects. However, the number of such defects is naturally dependent on system size—larger systems are statistically more likely to host a greater number of independent QLMs, in line with expectations for extensive disordered systems.

It is important to emphasise that, unlike an isolated QLM, a soft spot is defined based on the superposition of multiple low-frequency vibrational modes, and several soft spots can emerge simultaneously[20,22,23]. While low-frequency phononic modes contribute to soft spots by definition, their influence is limited due to their high participation ratios (*PR*). These observations suggest that each soft spot fundamentally originates from at least one underlying QLM. The microscopic architecture of soft spots—particularly their connection to specific QLMs—warrants further investigation. Consequently, the total number of soft spots in a glass is expected to scale with the number of QLMs, whether these modes act independently or are hybridised with phonons[34]. Moreover, our results imply that soft spots associated with particularly low-frequency QLMs may span larger spatial regions and exhibit enhanced susceptibility to external excitation.

In Fig. 3a2, b2, we highlight only the atoms with the highest values of Ψ_i (see below), revealing a consistent subset of particles that form the 'key core' of each QLM. These atoms are arranged in a one-dimensional, string-like configuration, indicative of a vibrational mode that can be excited with minimal volumetric displacement—a characteristic that is particularly favourable in densely packed systems.

Notably, we find no significant correlation between particle species and key-core participation as measured by Ψ_i. This lack of chemical selectivity suggests that the emergence of key-core defects is dictated predominantly by local mechanical environments, rather than by compositional or species-specific factors.

https://doi.org/10.1038/s41467-025-60781-7

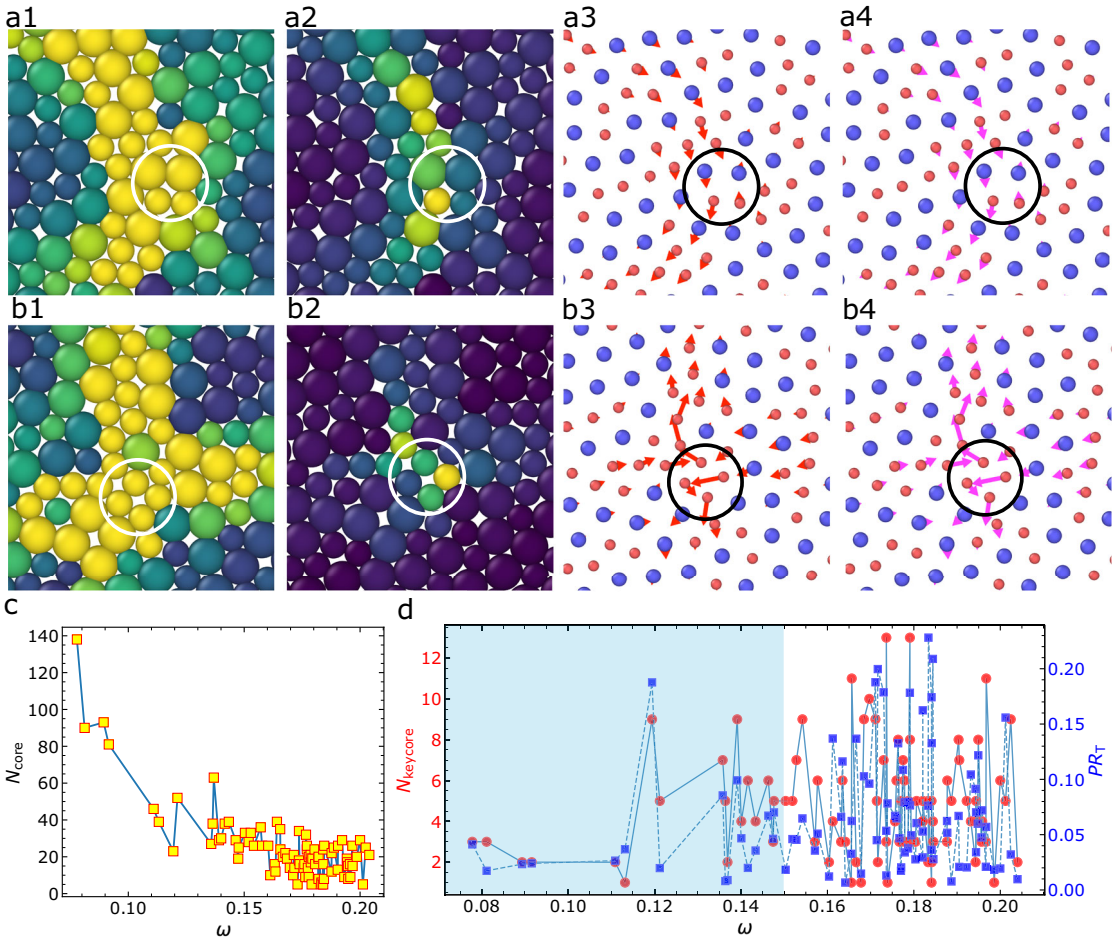

Fig. 3 | Correlation among vibrability, eigenvector and non-affine displacement fields at the core of QLMs in 2DIPL. Panels **a1**–**a4**, **b1**–**b4** correspond to the QLMs shown in Fig. 2a, f, respectively. The two particle species are distinguished by size. **a1**, **b1** Spatial maps of vibrability Ψ_i, with high-Ψ atoms ($\Psi_i > 0.25$) highlighted in yellow to identify the QLM core (26 and 33 atoms, respectively). **a2**, **b2** Subset of the highest-Ψ atoms (bright yellow), revealing the 'key-core string' with a pronounced one-dimensional geometry. **a3**, **b3** Eigenvector fields of the lowest-frequency vibrational modes. Atoms with higher Ψ_i values show longer vectors aligned along the string-like direction. Full fields are shown in Fig. 2a, f. **a4**, **b4** Non-affine displacement fields induced by minimal strain (simple shear in **a4**, compression in **b4**), closely reproducing the eigenvector field patterns. Vector lengths are rescaled for clarity. **c** Mode frequency (ω) dependence of the number of core atoms ($\Psi_i > 0.25$), N_{core}, sampled over an ensemble of systems. **d** Frequency dependence of the number of atoms forming the key core, $N_{keycore}$ (red circles), and the transverse participation ratio, PR_T (blue squares). The shaded region denotes the QLM-dominated regime with minimal phonon coupling.

Examining the eigenvector field in Fig. 3a3, b3, we see that the direction of atomic displacement aligns with the string structure, facilitated by the lack of nearby particles along the vibration direction. Consistent with our earlier discussion, the non-affine displacement field in Fig. 3a4, b4 faithfully reproduces the features of the eigenvector field. This establishes a robust connection between vibrability, eigenvector field characteristics, and plastic deformation.

Notably, despite the string-like structure at the core of a four-leaf-type QLM, its vibrational behaviour is characterised by substantial volume changes. This is evidenced by pronounced longitudinal components in the eigenmode, as shown in Fig. 1c, d. These volumetric vibrations originate from the intrinsic fourfold symmetry formed by four central particles arranged in a square configuration—termed the 'key-core square' (see circled regions in Fig. 3a, b). A detailed, quantitative characterisation of the key-core square, including its geometric alignment and two-in, two-out vibrational symmetry, is provided in the Methods section, with illustrative examples presented in Supplementary Fig. 4.

This structure represents the microscopic origin of mechanical frustration within the glass matrix and closely resembles an Eshelby-type inclusion[57], which simultaneously produces localised volumetric strain and a long-range shear field. Surrounding the key-core square, a string of particles with elevated vibrability naturally emerges. This string-like vibration arises from nearby particle arrangements that permit low-energy, one-dimensional vibrational motion—especially favourable in densely packed configurations. We refer to this particle string with large vibrability as a 'key-core string'. The presence of this string serves as both a signature of the defect core and a pathway for mechanical energy localisation. These key-core square and string are embedded within an unstable soft core region characterised by disordered volumetric fluctuations.

To effectively pinpoint the key core string of these QLMs in different glass samples, we come up with a simple empirical criterion: $\Psi_i > 60\% \cdot \max_i(\Psi_i)$. Although this cutoff is not deterministic—since Ψ_i is a continuous variable—it effectively isolates the key core, as illustrated in Fig. 3a2, b2. This will be further validated in the following sections.

For samples where QLMs emerge as the lowest-frequency mode in the large ensemble (see Supplementary Fig. 1), we present the size of the key-core strings, denoted as $N_{keycore}$, depending on ω, alongside their corresponding transverse part of participation ratio (PR_T) in Fig. 3d (see Supplementary Fig. 5 for the total and longitudinal participation ratios). This visual representation vividly captures the synchronised fluctuations of $N_{keycore}$ and PR_T as a function of ω in the light-

blue shaded region, where QLMs is free from coupling to phonons. This revelation adds physical significance to *PR*, extending beyond its conventional role of distinguishing phonons from QLMs. Furthermore, it underscores the robust localisation of these QLMs, even in the presence of far-field power-law decay features.

We note that Ψ and PR_T characterise different but complementary aspects of low-frequency QLMs. The field Ψ quantifies the local vibrational susceptibility, capturing the total amplitude of atomic motion− including both longitudinal (volumetric) and transverse (shear) components−making it particularly effective in identifying the core of soft modes. In contrast, PR_T serves as a global metric, indicating the degree of spatial delocalisation specifically associated with the transverse part of a given mode. Figure 3d suggests that QLMs with more extended key-core strings tend to exhibit larger transverse participation, contributing to a higher PR_T. This implies that while Ψ highlights local excitability, particularly near the defect core where longitudinal activity dominates, PR_T reflects how far the transverse (shear-related) influence of the mode extends across the system. In this sense, the two measures offer complementary insight into the internal structure of QLMs: Ψ resolves the intensity and localisation of excitation, whereas PR_T captures the directional extent and delocalisation of transverse response.

Furthermore, as shown in Fig. 1b–d, the transverse component of the eigenmode (Fig. 1b) exhibits a strong spatial resemblance to the Ψ field (Fig. 1d), particularly in the regions beyond the core. Meanwhile, the longitudinal component (Fig. 1c) more clearly reveals the core itself. This visual comparison underscores the hybrid nature of QLMs: they feature both shear-driven and volumetric signatures, with a core dominated by compressive or dilational motion and a surrounding field shaped by long-range shear deformation.

Consequently, a QLM exhibits four distinct structural features: a localised key-core square, a surrounding key-core string, an unstable soft core region characterised by longitudinal vibrational components, and a stable, long-range four-leaf-type shear strain field. The soft core region may correspond to what are commonly referred to as soft spots in disordered solids.

Interestingly, the size of the key-core string, $N_{keycore}$, does not directly correlate with the size of the soft core, N_{core}, as illustrated in Fig. 3c, d. This decoupling suggests that the structural origin of QLMs involves a more complex interplay between localised defects and the surrounding disordered matrix than previously assumed.

While the mechanisms governing N_{core} remain somewhat unclear, its variation may reflect the system's capacity to absorb volumetric deformations within a disordered environment. Specifically, a large value of N_{core} implies that the volume fluctuations induced by the two-in, two-out vibration of the key-core square are more effectively accommodated by the surrounding particles. This enhanced ability to accommodate deformation−enabled by local mechanical softness−reduces the mechanical energy cost of excitation, thereby lowering the mode frequency ω, as observed in Fig. 3c.

In contrast, crystalline solids lack this volumetric compensation due to their rigid, ordered structure. As a result, QLMs in crystals exhibit minimal soft core sizes, reinforcing the notion that structural disorder plays a central role in enabling energy localisation and mechanical softness.

These insights underscore the pivotal role of the key-core defect and its immediate environment in shaping the spatial extent and energetic characteristics of QLMs, ultimately defining their function as mechanically relevant excitations in disordered systems.

Finally, motivated by recent developments in the study of topological defects in disordered systems[26–28], we perform a topological characterisation of the eigenmodes shown in Fig. 2a, f. The analysis follows established procedures, with full methodological details provided in Supplementary Note 1. In addition to the full eigenmodes, we also apply the same analysis separately to their transverse and longitudinal components. Interestingly, in both cases, a persistent negative topological defect consistently appears at the centre of the four-leaf pattern, aligning with the core region of the QLM. However, numerous additional topological defects are detected in peripheral regions where vibrational amplitudes are negligible (see Supplementary Fig. 6). Notably, the longitudinal component−despite having much smaller overall amplitude than the transverse part−exhibits a larger number of topological defects. This discrepancy arises because the definition of topological defects relies solely on the orientation of eigenvectors−regardless of their magnitude. These observations suggest only a partial spatial overlap between topological defects and the mechanically defined key-core defects identified in this work. This distinction may help explain the absence of a strict one-to-one correspondence between topological defects and plastic events, as reported in prior studies[26].

Shear anisotropy induced by hierarchical defects

We now aim to establish a link between the identified localised defects and the mechanical properties. The dominant role of the transverse component in the eigenmode suggests a significant role of the shear modulus associated with the QLMs. A QLM can lead to shear anisotropy and softening. Therefore, we focus on the simple shear modulus *G*.

Due to the spatial variation in the orientation of QLMs, as demonstrated above, relying solely on the horizontal direction of shear deformation may not adequately capture shear modulus anisotropy. To address this, we measure the orientation-dependent shear modulus $G(\theta)$ using the approach introduced in ref. 58. Here, θ denotes the clockwise rotation angle of the sample's horizontal axis relative to its original orientation.

We identified two typical cases in glassy solids, as illustrated in Figs. 4, 5. These examples correspond to the cases discussed earlier in Figs. 2, 3. Additional examples are shown in Supplementary Figs. 7, 8.

In general, $G(\theta)$ exhibits substantial angular dependency, which varies among different samples. By comparing the eigenvector field of the QLM with $G(\theta)$, we observe that the reduction in $G(\theta)$ towards the weakest orientation and the rate of decline are influenced by the characteristics of the QLMs. Notably, the smallest $G(\theta)$ corresponds to the minimal phonon velocity, and this orientation-dependent phonon velocity can render the separation of QLMs from phonons, based on phonon velocities estimated from macroscopic shear modulus measurements, unreliable.

Figure 4 illustrates the microscopic features corresponding to the QLM in Fig. 2a. Significant shear softening and shear anisotropy are evident from $G(\theta)$, as shown in Fig. 4a (inside light-blue curve). This anisotropic response to mechanical stimuli has been experimentally observed in metallic glasses[54].

We present the excited atoms (cyan) with large non-affine displacements in the strongest direction (~45°) and the weakest direction (~90°) in Fig. 4b1, c1, respectively. At $\theta = 45°$, the QLM is not excited, and only a minor secondary string is activated (cyan particles in Fig. 4b1). In contrast, at $\theta = 90°$, the QLM is significantly excited, with no other strings activated, as shown in Fig. 4c1. This observation explains the shear softening observed in different directions. By pinning the key-core string atoms of the QLM (yellow atoms in Fig. 4b2, c2), we find that the excited atoms at $\theta = 45°$ remain largely unchanged (compare Fig. 4b2 with Fig. 4b1). In contrast, pinning at $\theta = 90°$ fully suppresses the non-affine deformation from the QLM, with only minor secondary strings (cyan particles in Fig. 4c2) taking up the shear strain. The full non-affine displacement fields are shown in Supplementary Fig. 9 (see Supplementary Movies S1,S2 illustrating the orientation-dependent excitation of the QLM in glasses with and without atomic pinning, respectively).

When we measure $G(\theta)$ with the key-core string or key-core square atoms pinned, the shear softening and shear anisotropy are greatly

https://doi.org/10.1038/s41467-025-60781-7

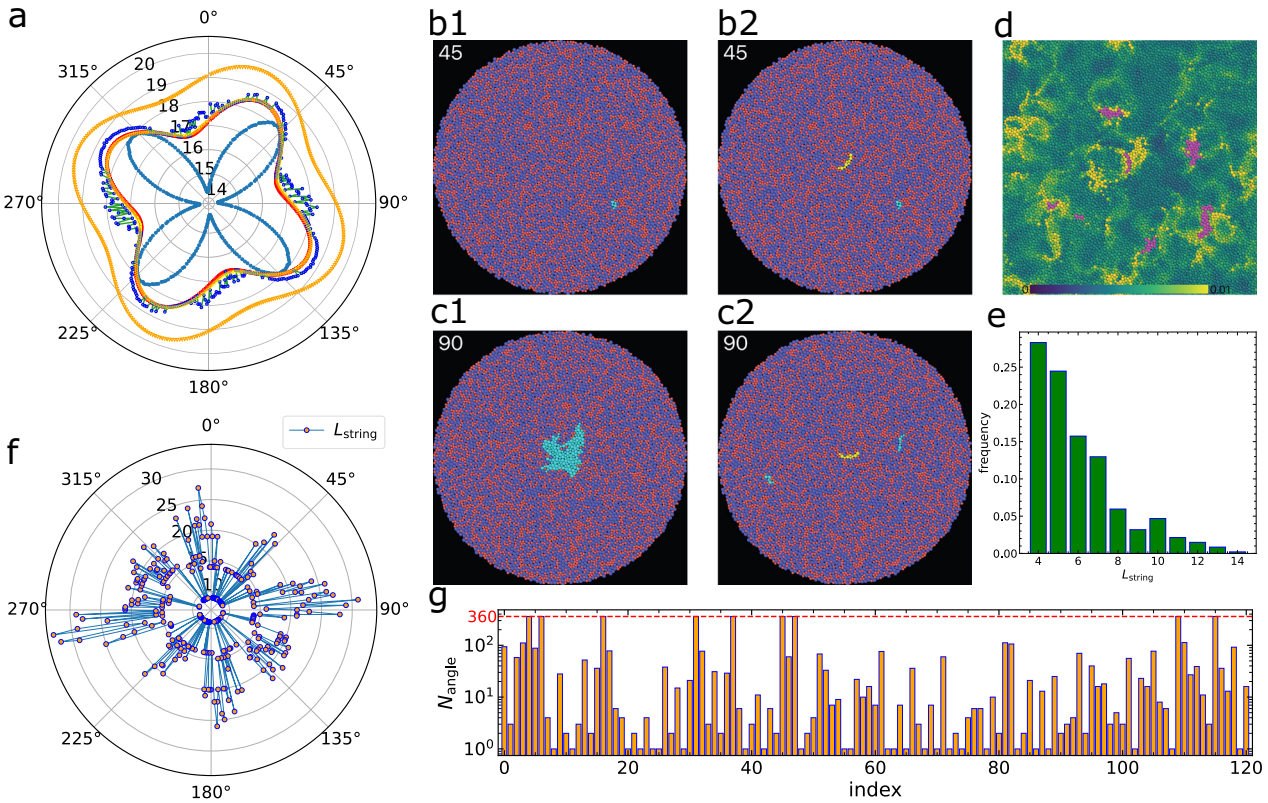

Fig. 4 | Shear anisotropy induced by hierarchical QLMs. a Angular dependence of the simple shear modulus $G(\theta)$ in polar coordinates for the system shown in Fig. 2a. Five measurements are shown, from inner to outer: (light blue) unpinned system; (red) with key-core string atoms pinned (yellow atoms in **b2**); (yellow, nearly overlapped with red) with only key-core square atoms pinned; (blue) with both key-core atoms and θ-dependent strings pinned (yellow and cyan atoms in **c2,** $\theta = 90^{\circ}$); (orange) with key-core atoms and all hidden strings pinned (magenta atoms in **d**). **b1**, **c1** Excited atoms (cyan) with large non-affine displacements at $\theta = 45^{\circ}$ (**b1**) and 90° (**c1**) when no pinning is applied. **b2**, **c2** Same configurations after pinning the key-core atoms (yellow), showing suppression of the primary QLM at $\theta = 90^{\circ}$ (**c2**) but not at $\theta = 45^{\circ}$ (**b2**). **d** Spatial distribution of reduced transverse vibrational density of states, $D_i^{\mathrm{T}}(\omega)/\omega$ for $\omega = 0.8 \pm 0.4$. Magenta atoms represent the union of the key-core and θ-dependent string excitations. **e** Length distribution of θ-dependent strings with $L_{\mathrm{strings}} > 3$, showing a rapid decay in string length. **f** Angular dependence of the number of atoms participating in the key-core and hidden strings. This curve maps closely onto the anisotropy observed in $G(\theta)$ (compare with blue curve in **a**). **g** Frequency of pinning occurrences for each magenta atom from (**d**), as the system is rotated in 1° increments over 360°. Atoms with $N_{\mathrm{angle}} = 360$ (horizontal red dashed line) are the key-core atoms that are always excited. Other atoms show orientation-specific excitation, confirming the directional nature of string-like defects.

reduced, as seen from the red or yellow curves in Fig. 4a, respectively. A closer examination reveals that pinning a key-core square is slightly more effective in reducing these effects, highlighting its critical importance. This outcome is expected, as only the key-core square exhibits two-in, two-out vibrations, which are responsible for the fourfold symmetry. The key-core string arises as a consequence of the key-core square and reflects the preference for one-dimensional vibrational excitations.

During shear deformation under atomic pinning, significant non-affine displacements are realised by string-like atom chains, such as those shown in Fig. 4c2. These secondary strings have much higher activation energy than the primary QLM at the centre and can be selectively excited depending on θ. We visualise all the excited strings at 0°–360°, including the key core string, as magenta particles in Fig. 4d. Despite their excitation at different angles, these strings largely overlap spatially (see Supplementary Movies S1, S2), obscuring their string-like feature in Fig. 4d. This suggests the existence of hidden defects that depend on the system's structure and may vary with different glass states. Interestingly, Fig. 4d shows that these magenta atoms nearly overlap with the atoms exhibiting a large reduced transverse density of states at low frequencies, below the boson peak[40].

Additional analyses of these hidden strings reveal the length distribution of strings with more than 3 particles, as shown in Fig. 4e. The data indicate a rapid decay in the number of strings as their length increases, suggesting that shorter strings are generally more prevalent, especially among those that can be excited by minimal strain. This trend is intuitive, as longer strings require more specific particle arrangements to support one-dimensional particle motion. The angular (θ-) dependence of the number of particles in a string, L_{string}, for all strings in the system, as shown in Fig. 4f, closely mirrors the shape of $G(\theta)$ measured without atomic pinning.

In general, higher rigidity in a solid corresponds to a lower density of defects. The angular distribution of defect-associated atoms shows clear peaks near $\theta = 0^{\circ}$, 90°, 180° and 270°—precisely the directions where $G(\theta)$ exhibits the most pronounced softening in the unpinned system. This alignment supports the view that directional excitation of string-like defects plays a key role in mechanical softening. The observed correlation between $L_{\mathrm{string}}(\theta)$ and $G(\theta)$ thus reinforces our claim that the anisotropic mechanical response is rooted in the θ-dependent activation of these defects. This similarity further indicates that these hidden secondary string-like defects, together with the key-core square and string structures, significantly contribute to shear softening.

Repeating the atomic pinning process by also pinning particles in the angle-dependent string at each θ (Fig. 4f), we measure a new $G(\theta)$, depicted by the blue dot in Fig. 4a. This operation (blue dots) reduces shear anisotropy but remains comparable to the red curve. On the

https://doi.org/10.1038/s41467-025-60781-7

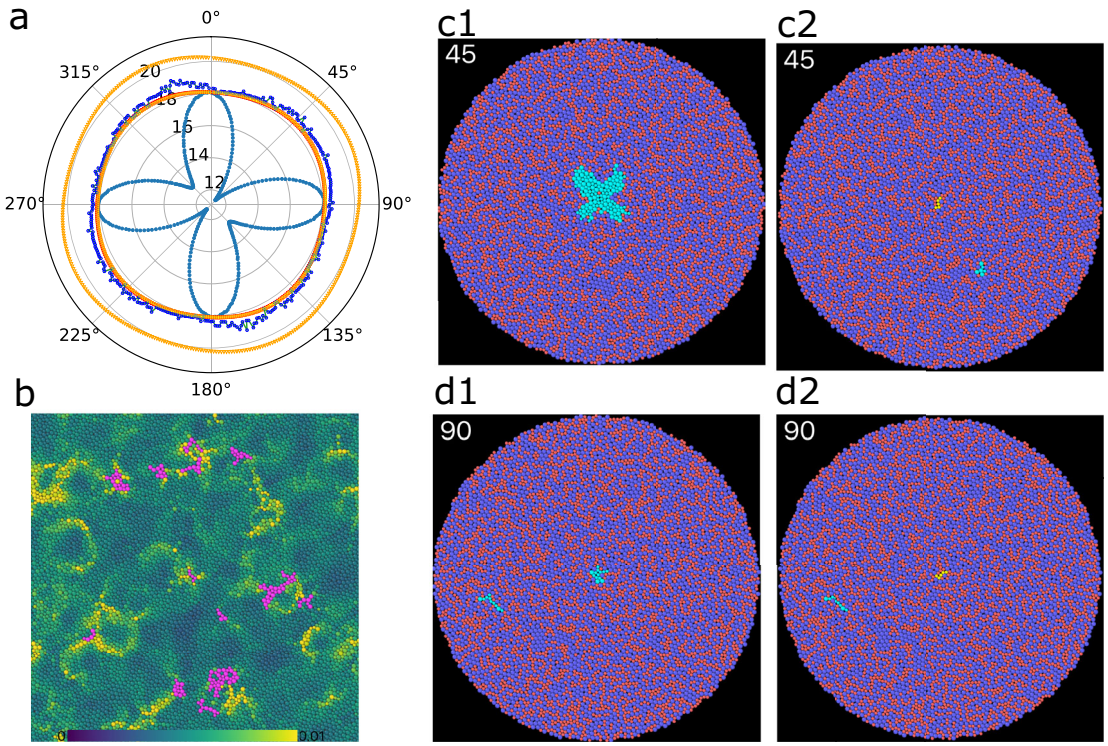

Fig. 5 | Shear anisotropy induced by a primary QLM. a $G(\theta)$ in polar coordinates for the system in Fig. 2f. The colour scheme in (**a**) and the atomic colouring strategy in other panels are consistent with those in Fig. 4. **b** Particle-level reduced transverse density of states, $D_i^{\mathrm{T}}(\omega)/\omega$, for $\omega = 0.8 \pm 0.4$. The magenta atoms represent the union of θ − dependent strings and the key core atoms. **c** Atomic configurations at $\theta = 45^{\circ}$ with excited atoms marked as cyan when the key core atoms unpinned (**c1**) or pinned (yellow atoms) (**c2**). **d** Atomic configurations at $\theta = 90^{\circ}$ similar to (**c**) when the key core atoms unpinned (**d1**) or pinned (**d2**).

other hand, pinning all magenta particles in Fig. 4d and measuring $G(\theta)$ results in the outer orange curve in Fig. 4a, showing a significant reduction in shear anisotropy. The remaining anisotropy may be due to defects undetected with the cutoff in the non-affine displacements, i.e. weaker contributors not included in the analysis. We propose that the hierarchical nature of defects in glasses, which display continuous variations in activation energies and strain responses, arises as a consequence of the underlying structural disorder.

From all strings in the system, including both the key core and hidden defects, totalling 121 particles (visualised in Fig. 4d), we plot the number of times these atoms are pinned at different θ values (with a 1° step) in Fig. 4g. For instance, the key core atoms are consistently pinned, resulting in a value of 360. Atoms are pinned at each θ only when they are excited, without pinning, excluding the key core atoms, which are always pinned. Thus, pinning times inherently reflect excitation times. Many of these particles are excited at multiple angles, reflecting various string forms, further demonstrating the orientation sensitivity of string-like defect excitations in glasses, as highlighted by the curved arrangement of the key core atoms. This multiple excitability of string-like particles across different orientations explains why pinning them at a single angle does not substantially reduce the anisotropy in $G(\theta)$ (blue dots in Fig. 4a), when compared to the yellow and red curves.

Considering the association between four-leaf QLMs and soft spots, the orientation-dependent behaviour of QLMs—and consequently the shear modulus—naturally explains why not all soft spots are activated within a single plastic event. This anisotropy in soft spots highlights their diverse activation conditions, providing a valuable perspective for future research. Understanding this phenomenon could offer deeper insights into the mechanics of glassy materials and the nature of plastic deformation.

We now turn to the other typical case illustrated in Fig. 5, corresponding to the QLM in Fig. 2f. The shear softening and shear anisotropy observed from $G(\theta)$, represented by the inner light-blue curve in Fig. 5a, are pronounced, similar to the previous case, but in different directions from the one in Fig. 4a. As before, we examine the non-affine displacement fields under minimal shear deformation along the weakest ($\theta = 45°$) and strongest ($\theta = 90°$) directions, shown in Fig. 5c1, d1, respectively. Consistently, at $\theta = 45°$, the QLM is prominently excited, exhibiting a four-leaf pattern with no other atoms activated. Conversely, at $\theta = 90°$, the QLM is significantly suppressed, and a hidden secondary string is activated.

After pinning the key-core string (the yellow atoms in Fig. 5c2, d2), the QLM is completely suppressed, with only secondary strings remaining active. The full non-affine displacement fields for Fig. 5c1, c2, d1, d2 are presented in Supplementary Fig. 9.

More significantly, when examining $G(\theta)$ in Fig. 5a after pinning only the key-core square atoms composed of four atoms (circled atoms in Fig. 3b) or the key-core string particles, the shear anisotropy almost disappears (nearly overlapping yellow and red curves, respectively), rendering the system nearly isotropic—distinct from the previous case. We also extract all hidden strings and display them collectively in Fig. 5b as magenta particles. Pinning the angle-dependent strings in addition to the key-core atoms, individually or together, results in only a slight reduction in shear anisotropy, as indicated by the blue dots and orange curves in Fig. 5a. However, the amplitude of the shear modulus is increased when all particles are pinned.

We speculate that the significant difference from the case in Fig. 4 may be due to the substantially higher activation energy of the hidden strings compared to the key core ones in this case. Consequently, these hidden strings contribute less to shear instability at minimal strain. This variation underscores the inherent disordered structure of glasses, which creates a diverse distribution of local states with varying activation energies, leading to hierarchical defects. This implies that such defects are likely influenced by the thermal history of the sample.

Here, we note that these observations are also common to another system we studied, namely the 2DKA model. Representative results are presented in Supplementary Figs. 10, 11, demonstrating the broad applicability of our findings to systems with both repulsive and attractive interactions.

These observations highlight the critical role of the key-core square and string atoms at the centre of the most prominent QLM in determining both the four-leaf anisotropy of the QLM and the shear anisotropy. The highly localised nature of these key-core squares justifies their classification as 'defects in a glass'. Higher-order defects, composed of many hidden strings, have a minor yet non-negligible impact on the system's mechanical properties. The hierarchical nature of defects in glasses, stemming from underlying structural disorder, distinguishes them from defects in crystals (see below).

The results not only reinforce our assertion that the key-core square of the four-leaf-pattern QLMs acts as mechanical defects in glasses but also provide further evidence for the existence of soft spots potentially involving multiple QLMs. It is notable that the mechanical coupling of multiple QLMs could give rise to intriguing memory effects, as discussed in previous studies[59]. Additionally, the observed pinning effect highlights the crucial role of the string-like vibration's orientation in shaping the spatial characteristics of the four-leaf pattern. Further investigation is needed to explore the underlying physical mechanisms behind these phenomena.

Shear anisotropy triggered by QLMs in a defected crystal

The mechanical defect-like nature of the QLM's key core suggests that QLMs are not exclusive to glassy materials and could potentially exist in any system where space permits transverse motion, aligning with examples observed in crystals[38]. To investigate how structural disorder affects the occurrence of low-frequency QLMs, we performed simulations on a monatomic crystal with inherent point defects like vacancies (see Methods). This crystal, formed through slow cooling, demonstrates hexatic order with quasi-long-range positional and long-range orientational orders.

In the defected crystal with two vacancies, we begin by analysing the minimal-frequency vibration mode and decompose it into transverse and longitudinal components, following the same method used for glasses. Remarkably, the phononic mode is intricately coupled with two QLMs that exhibit characteristic four-leaf patterns. These QLMs are centred around the vacancies, setting them apart from soft spots in imperfect colloidal crystals, which do not effectively detect vacancies[25]. Figure 6a illustrates the transverse component, while the full eigenvector field and the longitudinal component can be found in Supplementary Fig. 12. Similar to the behaviour observed in glasses, the predominant component of the mode is transverse, though the longitudinal component is also significant. Notably, atoms participating in the four-leaf pattern consistently show more pronounced longitudinal components.

Simultaneously, the four-leaf pattern feature aligns well with the atomic-scale vibrability Ψ_i (see Fig. 6b and Supplementary Fig. 12). This highlights Ψ's effectiveness in identifying crystal defects, just as in amorphous systems.

To investigate the mechanical properties of QLMs in a manner similar to our glass studies, we apply four distinct deformation protocols to excite them. Due to the specific orientation of the QLMs, all four deformation methods can activate them, albeit to different degrees (see Supplementary Fig. 12d1–d4). The resulting non-affine displacement fields consistently reflect the characteristics of the QLMs observed in the eigenvector field.

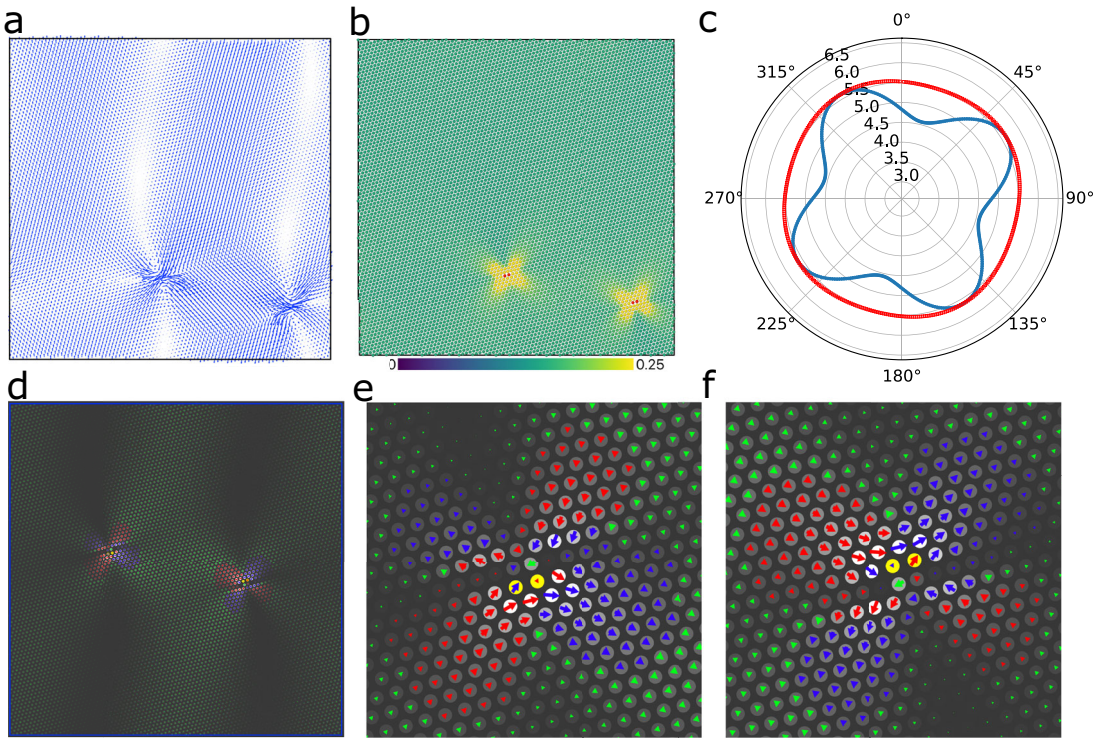

Fig. 6 | Vibration modes and the associated shear anisotropy of a monatomic crystal model with defects. a The transverse component of the minimal-frequency vibration mode, with an amplitude of 0.968. **b** Visualisation of the atomic-scale vibrability Ψ_i. The two vacancy defects are indicated by the four red particles. **c** $G(\theta)$ of the defected crystal in polar coordinates. The inner blue curve illustrates $G(\theta)$ in the normal (unpinned) state, while the outer red curve shows $G(\theta)$ with the four key core atoms (see **b**) pinned. **d** The divergence ($\nabla \cdot \mathbf{u}_i^{np}$) field of the net-projection vectors (arrows) of the eigenvector. The QLMs have been shifted to the centre for better visualisation. Blue and red indicate negative and positive divergence, respectively, while green represents nearly zero divergence. The divergence patterns resemble intricate butterfly shapes. Panels (**e**, **f**) provide enlarged views of the left and right QLMs in (**d**), respectively. The yellow atoms at the centre are the key core atoms, corresponding to the red ones in (**b**).

We further perform an eigenvector projection analysis (see Methods), specifically targeting the QLMs. The resulting projection product accurately captures the vector characteristics, with its divergence field showing non-zero values at the QLM cores (see Fig. 6d–f). Interestingly, the regions surrounding the vacancy display either positive or negative divergence, indicating the presence of volumetric deformations.

Notably, the atoms with the largest Ψ_i values, especially around the vacancy, define the location of the QLMs, displaying a gradient with a string-like feature. This observation is consistent for both QLMs, as illustrated in the enlarged views in Supplementary Fig. 13a, d. The eigenvector direction of the QLM aligns consistently with this string structure (see Supplementary Fig. 13b, e). Remarkably, the non-affine displacement fields from all deformation protocols exhibit features similar to those of the eigenvector field. As observed in glasses, the vector directions are opposite between the simple shear and between tension and compression (see Supplementary Fig. 13c, f).

Adopting a methodology similar to that used for glasses, we focused on four key core atoms within the crystal (red particles in Fig. 6b) and investigated their impact on mechanical properties using atomic pinning. First, we analysed $G(\theta)$ in the unpinned original system (see Fig. 6c). This analysis reveals a significant and pronounced anisotropy, with the direction of the weakest shear modulus, $G(\theta)$, determined by the orientation of the QLM's key core, while the remaining atoms are positioned within the perfect lattice. Pinning these four key core particles reduces the observed anisotropy in $G(\theta)$ to nearly negligible levels, resulting in a significantly stiffer and more isotropic matrix (see Supplementary Movies S3, S4 for the orientation-dependent non-affine displacement field).

The findings from the defective crystal studies indeed reinforce the view that QLMs are fundamental dynamical defects across different material types. Their behaviour as force dipoles and the consistent presence of key-core squares and strings highlight their significant role in both crystalline and amorphous materials. This broadens our understanding of how such defects influence mechanical properties and highlights their relevance for various applications and material designs.

Discussion

To summarise, we have investigated mechanical defects by examining low-frequency quasi-localised modes (QLMs) in both amorphous and crystalline solids. Our study reveals a hierarchical underlying structure of QLMs. First, we have confirmed that a QLM comprises a roughly circular-shaped core surrounded by a long-range shear strain field[33,36]. At the centre of this large core, we identify a key-core square formed by four particles, along with a key-core string. The key-core square exhibits a two-in, two-out vibration pattern at the particle level, generating long-range shear strain fields with fourfold symmetry. The volumetric (or longitudinal) vibrations induced by the key-core square are contained within the core, which is sufficiently large for the matrix to accommodate volume deformation. When local particle arrangements allow for one-dimensional vibrations, the key-core string is activated by the two-in, two-out vibrations of the key-core square. This string can be detected by analysing particles with high atomic-scale vibrability. Once the key-core string is identified, the key-core square can be further characterised through its distinct two-in, two-out vibration pattern.

The key-core square affects non-affine displacements, shear softening, and shear anisotropy in its vicinity. Its localised nature identifies it as a microscopic defect in glasses. The consistent role of the key-core square in both glasses and crystals indicates that it represents a universal core structure linked to energy dissipation, irrespective of whether the material is structurally ordered or disordered.

In addition to the strongly localised key-core square and string found in primary QLMs, we identify defects with higher excitation energies. Unlike the primary defects, these higher-energy defects do not have a single distinct string; instead, their cores consist of multiple strings. This observation highlights the hierarchical nature of defects in glasses, a characteristic arising from structural disorder that is not present in crystals.

Despite their apparent similarities, it is important to note that the key-core strings of QLMs are distinct from the strings responsible for the boson peak. The key difference lies in the presence of fourfold volumetric deformations in QLMs, reflecting their two-in-two-out vibrational feature. In contrast, the stringlets related to the boson peak do not exhibit these fourfold deformations[40]. Additionally, these key-core strings may differ from the string-like motions induced by (quasi-) voids, which are involved in structural relaxation[60]. String-like motions are most easily excitable in densely packed systems. Understanding the intrinsic differences among these string-like features, which impact glass properties across various length and time scales, is essential for advancing future studies[40,60–63].

QLMs are widely recognised as the possible origin of two-level tunnelling systems, as discussed in Ref. 2. Given the significant energy difference between the boson peak and QLMs, it is tempting to propose that the key cores of QLMs primarily contribute to the formation of two-level tunnelling systems, whereas the stringlets identified in ref. 40 are responsible for the boson peak. We thus propose that these two distinct defect types underpin different classes of nonphononic vibrational excitations in glasses.

Our findings indicate that QLMs result from particle-level localised defects, even though they are associated with a long-range strain field. This indicates that the four-leaf-type primary QLMs could be a common feature in both crystals and glasses. Interestingly, recent research[64] shows that hyperuniform glasses—considered mechanically self-organised and defect-free at a high level[65]—lack low-frequency QLMs. This observation supports our hypothesis that QLMs do not originate from structural disorder but rather from mechanical frustration. Consequently, we propose that the key-core square of a QLM should be regarded as a type of 'localised mechanical defect' in glasses, highlighting the importance of mechanical defect concepts even in structurally disordered amorphous materials.

At finite temperatures, thermal fluctuations can obscure the features of soft vibrational modes, making it more challenging to directly observe QLMs—particularly their spatial symmetry and localisation[66,67]. Nonetheless, we expect that techniques such as time-averaged dynamical structure analysis, frequency-domain filtering, or reconstructions based on the underlying energy landscape could still enable the identification of key-core defects, especially in the low-temperature regime. A quantitative exploration of these approaches represents a promising avenue for future research, with the potential to bridge zero-temperature theoretical predictions and experimentally accessible observables.

The absence of QLMs in perfect crystals and hyperuniform glasses reinforces their connection to localised defects and highlights the potential for controlling their presence through materials processing, similar to managing structural defects in crystals. Experimental methods, such as long-time annealing, mechanical training, and ultrastable glass formation via physical vapour deposition, along with numerical techniques like the SWAP method or achieving hyperuniform states, can help eliminate QLMs. Understanding the emergence of low-frequency QLMs is crucial for understanding properties like plastic deformation in glasses. Further research is needed to explore these aspects in greater depth in future studies.

Recent studies on topological defects[26–28] have provided valuable insights into deformation mechanisms in glasses, particularly under finite-temperature or driven conditions. These works emphasise topological features extracted from non-affine displacement fields or vibrational mode orientations. In contrast, our study focuses on intrinsic particle-level defects identified at zero temperature from vibrational eigenmodes. Specifically, we define defects based on a

mechanically rooted criterion: a four-particle 'key-core' structure exhibiting a two-in, two-out symmetry in the lowest-frequency QLM. Unlike previous approaches relying on displacement patterns under strain or topological indicators, our defect is defined directly from the zero-temperature vibrational structure, offering a uniquely intrinsic, mechanical origin. This approach provides a mechanical perspective distinct from purely topological characterisations. Elucidating the potential connections between these mechanically defined key-core defects and topological defects remains an important and promising direction for future research.

In this work, our focus has been on identifying and characterising a single, intrinsic defect—the key-core structure—within glassy solids. However, understanding how these defects interact and evolve under external deformation is a crucial next step. Preliminary simulations under simple shear indicate that key-core defects are preferentially activated over a broad strain range and are strongly associated with plastic events involving stress drops (see Supplementary Note 2 and Supplementary Fig. 14). Moreover, their spatial organisation and possible hybridisation may correlate with the onset of shear localisation. A systematic investigation into their mutual interactions, spatiotemporal correlations, and potential percolation into macroscopic shear bands is therefore a compelling avenue for future work[29,30].

Our choice to employ simple interaction models, such as the Lennard-Jones (LJ) and inverse power-law (2DIPL) potentials, was deliberate—aimed at uncovering universal features of mechanical defects without the confounding effects of chemistry-specific interactions. The consistent behaviour observed across both the 2DIPL and 2DKA models suggests that key-core defects are generic features of disordered solids. While we anticipate that such defects will also appear in more realistic models, including those based on embedded-atom method (EAM) potentials or machine learning-based force fields, their detailed properties may depend sensitively on the many-body nature of the interactions. Starting from minimal models enables us to build a foundational understanding before tackling these complexities. Ongoing work is extending our analysis to advanced potentials to assess the emergence and characteristics of key-core defects in more realistic systems, with results to be reported in a forthcoming study.

Our study primarily focused on 2D systems, motivated by two key considerations: (1) the significantly enhanced spatial resolution afforded by 2D, which enables clear visualisation and identification of localised defect structures, and (2) the computational efficiency required to conduct large-scale ensemble simulations and detailed vibrational mode analyses in this exploratory phase. Nevertheless, extending these findings to three dimensions (3D) represents an exciting and important direction for future research. In our recent work[68], we have shown that QLMs and their associated key-core structures persist in 3D binary glasses. These 3D QLMs preserve the essential localised characteristics observed in 2D, although their spatial morphology is often more intricate and multipolar in nature. This added complexity poses challenges in rigorously characterising their geometrical symmetry and angular dependence within the full 3D configuration space. Despite these challenges, the 2D results presented here provide a crucial foundation for developing a mechanistic understanding of QLMs. They allow us to isolate and examine the microscopic origins and structural signatures of mechanical defects with high fidelity. This insight now serves as a guiding framework for our ongoing, technically intensive efforts to characterise and generalise these defects in 3D systems. Furthermore, investigating the relationship between these mechanically defined defects and the merged percolation scenario observed in 2D relaxation dynamics by Gao et al.[69] presents an intriguing avenue for future research.

Finally, our findings have significant technological implications. They reveal that even in structurally isotropic disordered amorphous systems, mechanical isotropy is not guaranteed in small finite-size regions. The mechanical properties of nanoscale amorphous materials, such as phase change materials that require rapid, reversible phase transformations, are heavily influenced by the presence or absence of QLMs or localised mechanical defects. Our discoveries provide new perspectives on how to effectively manage and control the mechanical properties of these materials at the nanoscale.

Looking forward, the ability to mechanically identify and suppress localised vibrational defects opens new routes for designing ultra-stable amorphous materials with tailored mechanical properties—critical for applications in nanodevices, memory materials, and beyond.

Methods

Molecular dynamics simulations

We use molecular dynamics simulations to investigate two distinct binary glass models and a monatomic crystal model, all in two dimensions. Periodic boundary conditions are applied in all simulations, and the *NVT* ensemble is employed. Throughout the simulation and analysis, reduced Lennard-Jones units are used.

One glass model interacts via the inverse power-law potential model (2DIPL):

$$U_{\alpha\beta}(r) = \epsilon\left(\sigma_{\alpha\beta}/r\right)^{10}, \tag{2}$$

where we set $\sigma_{AA} = 1.0$, $\sigma_{BB} = 1.40$, and $\sigma_{AB} = 1.18$ ($\alpha, \beta \in \{A, B\}$)[39,70]. The composition is 50:50. All mass m and the cohesive energy ϵ are set to 1.0. The potential and force are truncated and shifted to zero at $1.48\sigma_{\alpha\beta}$. We study a large ensemble of systems with $N = 8192$ atoms with a number density of $\rho = 0.86$. The glass transition temperature has been measured to be $T_g = 0.44$[39,40]. To obtain low-temperature glass states, we first melt and equilibrate the sample at high temperatures $T = 3.0$ and $T = 1.0$ for both $t = 4000$. Then the liquid is quenched to $T = 0.1$ at a cooling rate of 10^{-3}. The corresponding inherent structures are achieved by the conjugate gradient algorithm, after relaxing the glassy solids for a period of $t = 1000$.

The other glass model is the Kob-Andersen model (2DKA), where particles interact via a Lennard-Jones potential with a pair potential given by:

$$U_{\alpha\beta}(r) = 4\epsilon_{\alpha\beta}[\left(\sigma_{\alpha\beta}/r\right)^{12} - (\sigma_{\alpha\beta}/r)^6], \tag{3}$$

where $\alpha, \beta \in \{A, B\}$, $\sigma_{AA} = 1.0$, $\sigma_{BB} = 0.88$, $\sigma_{AB} = 0.8$, $\epsilon_{AA} = 1.0$, $\epsilon_{BB} = 0.5$, and $\epsilon_{AB} = 1.5$[41]. The potential and force are truncated and shifted at $r = 2.50\sigma_{\alpha\beta}$. The composition is 65:35 for better glass-forming ability. We study a large ensemble of systems with $N = 8192$ atoms with a number density of $\rho = 1.20$. The glass transition temperature has been reported to be around 0.33[41]. The low-temperature glass solids at $T = 0.1$ and their corresponding inherent structures are obtained in a similar procedure to the above. Different from the purely repulsive 2DIPL model, 2DKA includes long-range attractive interactions.

The crystal model also interacts similarly to the 2DIPL model but is a single-component system. We set all mass, cohesive energy, and particle size to be 1.0. The potential and force are truncated and shifted up to 1.48σ. We also consider a system of $N = 8192$ atoms with $\rho = 0.86$. To generate the natural crystal, we first melt and equilibrate the sample at $T = 2.0$ for $t = 2000$. Before energy minimisation, the sample is slowly quenched to $T = 0.01$ and relaxed for $t = 2000$.

We performed the following data analysis for the computer simulation configurations assisted by our home-developed open-source python package 'PyMatterSim'[71].

Vibration analyses

We characterise the vibrational properties of the glasses by directly diagonalising the Hessian matrix of the inherent structure. No negative

eigenvalue was found in any of our samples. The dynamical matrix is generally given by

$$D_{ij} = \frac{\partial^2 U}{\partial R_i \partial R_j}, \tag{4}$$

where R_i is the coordinate (x or y) of particle i. The participation ratio[1] of a vibrational mode is measured by

$$PR = \left(\sum_i^N |\mathbf{u}_i|^2\right)^2 / N \sum_i^N (\mathbf{u}_i \cdot \mathbf{u}_i)^2, \tag{5}$$

where $\mathbf{u}$ is an eigenvector.

Vibrational mode decomposition in real space

Each vibrational mode has been decomposed into the transverse and longitudinal components using a Volume matrix method[40,42]. This approach separates the modes based on their directional characteristics, allowing for a detailed analysis of the contributions of each component to the overall vibrational behaviour of the system. A matrix A is first built as

$$A_{i,j\alpha} = \frac{1}{V_i}\frac{\partial V_i}{\partial R_{j\alpha}}, \tag{6}$$

where V_i is the local volume of particle i. Then, an eigenvector $\mathbf{u}$ is projected to the transverse and longitudinal direction as $\mathbf{u}_\mathrm{L} = A^T(AA^T)^{-1}A\mathbf{u}$ and $\mathbf{u}_\mathrm{T} = \mathbf{u} - \mathbf{u}_\mathrm{L}$. The local volume is conserved for the transverse mode. After mode decomposition, we can calculate the corresponding PR for each component.

Eigenvector projection analysis

We employed a local eigenvector projection method to investigate the volumetric vibrational feature of the low-frequency QLMs. This process involves extracting the nearest neighbours of the central particle through Voronoi tessellation. Subsequently, we project the eigenvector of each neighbouring particle onto the positional vector between it and the central particle. The unit positional vector between particles i and j is denoted as $\mathbf{n}_{ij} = \mathbf{R}_{ij}/|\mathbf{R}_{ij}|$, and the projected component is $\mathbf{u}_j^{||} = (\mathbf{u}_j \cdot \mathbf{n}_{ij})\mathbf{n}_{ij}$. Finally, we compute the net projection onto the central particle as $\mathbf{u}_i^{\mathrm{np}} = \sum_j \mathbf{u}_j^{||} - \mathbf{u}_i$.

We further analyse the divergence field of the eigenvector projection product $\mathbf{u}_i^{\mathrm{np}}$. This calculation involves determining the divergence of the vector field defined by

$$\nabla \cdot \mathbf{u}_i^{\mathrm{np}} = \frac{1}{N_i}\sum_j^{N_i}(\mathbf{R}_j - \mathbf{R}_i)\cdot(\mathbf{u}_i^{\mathrm{np}} - \mathbf{u}_j^{\mathrm{np}}). \tag{7}$$

The presence of a non-zero value for $\nabla \cdot \mathbf{u}_i^{\mathrm{np}}$ signifies local volumetric movement.

Mechanical deformation protocols

To probe the dynamical nature of the QLMs, we perform athermal quasistatic deformations at minimal strain and investigate the induced non-affine displacement fields[72]. In this procedure, we first apply an affine deformation to the simulation box and then minimise the energy to bring the system to its inherent state. This allows us to measure the non-affine displacements of each particle. We employ four distinct deformation protocols: (1) simple shear along the positive horizontal axis, (2) simple shear in the reverse direction, (3) tensile deformation along the horizontal axis and (4) compression along the horizontal direction. The shear strain rate is $|\gamma_{xy}| = 3.0 \times 10^{-5}$, and the tensile/compressive strain rate is $|\gamma_{xx}| = 4.0 \times 10^{-5}$. These strain rates are very small compared to the macroscopic elastic response, allowing for a precise analysis of the non-affine displacement fields.

To measure the orientation-dependent shear modulus, we follow the methodology introduced in Ref. 58. This method has also been shown to be effective in studying the orientation-dependent plastic susceptibility in amorphous solids[73]. The procedure is as follows: Starting from the inherent structure of a glassy state, we isolate a circular region with a diameter of (L − 3.0) (L: box length) and remove the atoms outside this region. Then, we rotate the sample by an angle of θ clockwise in steps of 1°. This rotation does not affect the overall potential energy of the system. The outer layer of the sample, with a thickness of 2.0, is fixed in place to prevent any movement. Only affine deformations are permitted in this outer layer. The rest of the sample undergoes athermal quasistatic shear along the positive horizontal axis. We then calculate the shear stress and strain to determine the orientation-dependent shear modulus, $G(\theta)$, for each angle θ.

Quantitative characterisation of the key-core square

To ensure an objective and reproducible identification of the key-core square, we propose a quantitative approach that integrates both vibrability and eigenvector field information. Our method leverages the characteristic flow structure of the vibrational field, where the key-core square resides at a location where incoming flows from different directions converge, creating a strong cancellation effect—a defining feature of the two-in, two-out symmetry. The identification proceeds in two main steps:

(i) Locating the key-core string: We begin by applying a vibrability threshold, selecting particles that satisfy $\Psi_i > 60\% \cdot \max(\Psi_i)$. This criterion isolates atoms with the highest susceptibility to low-frequency excitation, thereby defining the key-core string. This subset serves as the candidate region for further identifying the key-core square.

(ii) Defining the key-core square: Within the key-core string, we construct a local force network. For each atomic pair, we calculate a normalised pair force defined as $f_{ij}/\langle f_{\alpha\beta}\rangle$, where f_{ij} is the pairwise force between particles i and j, and $\langle f_{\alpha\beta}\rangle$ is the mean force between atoms of types α and β. Very weak bonds are excluded to retain only physically meaningful local structures.Among the resulting candidate four-particle clusters, we select the key-core square based on two quantitative criteria:

1. Maximising string inclusion: the selected square should contain as many particles from the key-core string as possible.
2. Maximising vibrational cancellation: we define a cancellation metric

$$\Delta\mu = ||(\sum|\boldsymbol{\mu}_i|)|| - ||(\sum\boldsymbol{\mu}_i)||,$$

where $\boldsymbol{\mu}_i$ is the local polarisation vector of particle i within the candidate square. A larger $\Delta\mu$ indicates stronger cancellation of local vibrational directions, characteristic of the two-in, two-out configuration.This two-step framework captures the physically intuitive notion that the key-core square marks the convergence point of vibrational flow, where opposing directions meet and cancel. Such cancellation cannot be captured by arbitrary four-particle combinations. Representative examples illustrating the application of this method are provided in Supplementary Fig. 4.

Data availability

All data that support the findings of this study are available in the article and the Supplementary Information. The source data have been deposited in figshare at https://doi.org/10.6084/m9.figshare.29176472.v1.

Code availability

All codes used for simulation and analysis are available from the corresponding authors upon request. The source code used for data

analysis is available from PyMatterSim (https://doi.org/10.6084/m9.figshare.29176556.v1).

References

1. Allen, P. B., Feldman, J. L., Fabian, J. & Wooten, F. Diffusons, locons and propagons: character of atomic vibrations in amorphous Si. *Philos. Mag. B* **79**, 1715–1731 (1999).
2. Lerner, E. & Bouchbinder, E. Low-energy quasilocalized excitations in structural glasses. *J. Chem. Phys.* **155**, 200901 (2021).
3. Zeller, R. C. & Pohl, R. O. Thermal conductivity and specific heat of noncrystalline solids. *Phys. Rev. B* **4**, 2029–2041 (1971).
4. Krishnan, R. S. The scattering of light in fused quartz and its Raman spectrum. *Proc. Indian Acad. Sci.* **37**, 377–384 (1953).
5. Jäckle, J. On the ultrasonic attenuation in glasses at low temperatures. *Z. Physik.* **257**, 212–223 (1972).
6. Buchenau, U. et al. Low-frequency modes in vitreous silica. *Phys. Rev. B* **34**, 5665–5673 (1986).
7. Malinovsky, V. K. & Sokolov, A. P. The nature of boson peak in Raman scattering in glasses. *Solid State Commun.* **57**, 757 – 761 (1986).
8. Nakayama, T. Boson peak and terahertz frequency dynamics of vitreous silica. *Rep. Prog. Phys.* **65**, 1195 (2002).
9. Scalliet, C., Berthier, L. & Zamponi, F. Nature of excitations and defects in structural glasses. *Nat. Commun.* **10**, 5102 (2019).
10. Khomenko, D., Reichman, D. R. & Zamponi, F. Relationship between two-level systems and quasilocalized normal modes in glasses. *Phys. Rev. Mater.* **5**, 055602 (2021).
11. Zhou, Z.-Y., Yang, Q. & Yu, H.-B. Toward atomic-scale understanding of structure-dynamics-properties relations for metallic glasses. *Prog. Mater. Sci.* **145**, 101311 (2024).
12. Yu, H.-B., Gao, L., Gao, J.-Q. & Samwer, K. Universal origin of glassy relaxation as recognized by configuration pattern matching. *Natl. Sci. Rev.* **11**, nwae091 (2024).
13. Klinger, M. I. Atomic quantum diffusion, tunnelling states and some related phenomena in condensed systems. *Phys. Rep.* **94**, 184–312 (1983).
14. Galperin, Y. M., Karpov, V. G. & Kozub, V. I. Localized states in glasses. *Adv. Phys.* **38**, 669–737 (1989).
15. Buchenau, U., Galperin, Y. M., Gurevich, V. L. & Schober, H. R. Anharmonic potentials and vibrational localization in glasses. *Phys. Rev. B* **43**, 5039–5045 (1991).
16. Buchenau, U. Soft localized vibrations in glasses and undercooled liquids. *Philos. Mag. B* **65**, 303–315 (1992).
17. Buchenau, U. et al. Interaction of soft modes and sound waves in glasses. *Phys. Rev. B* **46**, 2798–2808 (1992).
18. Argon, A. S. Mechanisms of inelastic deformation in metallic glasses. *J. Phys. Chem. Solids* **43**, 945–961 (1982).
19. Falk, M. L. & Langer, J. S. Dynamics of viscoplastic deformation in amorphous solids. *Phys. Rev. E* **57**, 7192 (1998).
20. Manning, M. L. & Liu, A. J. Vibrational modes identify soft spots in a sheared disordered packing. *Phys. Rev. Lett.* **107**, 108302 (2011).
21. Smessaert, A. & Rottler, J. Structural relaxation in glassy polymers predicted by soft modes: a quantitative analysis. *Soft Matter* **10**, 8533–8541 (2014).
22. Chen, K. et al. Measurement of correlations between low-frequency vibrational modes and particle rearrangements in quasi-two-dimensional colloidal glasses. *Phys. Rev. Lett.* **107**, 108301 (2011).
23. Ding, J., Patinet, S., Falk, M. L., Cheng, Y. & Ma, E. Soft spots and their structural signature in a metallic glass. *Proc. Natl. Acad. Sci. USA* **111**, 14052–14056 (2014).
24. Fan, H., Fan, Z., Liu, X., Lu, Z. & Ma, E. Atomic vibration as an indicator of the propensity for configurational rearrangements in metallic glasses. *Mater. Horiz.* **8**, 2359–2372 (2021).
25. Chen, K. et al. Phonons in two-dimensional soft colloidal crystals. *Phys. Rev. E* **88**, 022315 (2013).
26. Wu, Z. W., Chen, Y., Wang, W.-H., Kob, W. & Xu, L. Topology of vibrational modes predicts plastic events in glasses. *Nat. Commun.* **14**, 2955 (2023).
27. Vaibhav, V. et al. Experimental identification of topological defects in 2D colloidal glass. *Nat. Commun.* **16**, 55 (2025).
28. Bera, A. et al. Clustering of negative topological charges precedes plastic failure in 3D glasses. *PNAS Nexus* **3**, pgae315 (2024).
29. Şopu, D., Stukowski, A., Stoica, M. & Scudino, S. Atomic-level processes of shear band nucleation in metallic glasses. *Phys. Rev. Lett.* **119**, 195503 (2017).
30. Şopu, D. et al. From elastic excitations to macroscopic plasticity in metallic glasses. *Appl. Mater. Today* **22**, 100958 (2021).
31. Giannini, J. A., Richard, D., Manning, M. L. & Lerner, E. Bond-space operator disentangles quasilocalized and phononic modes in structural glasses. *Phys. Rev. E* **104**, 044905 (2021).
32. Kapteijns, G., Richard, D. & Lerner, E. Nonlinear quasilocalized excitations in glasses: true representatives of soft spots. *Phys. Rev. E* **101**, 032130 (2020).
33. Richard, D., Kapteijns, G., Giannini, J. A., Manning, M. L. & Lerner, E. Simple and broadly applicable definition of shear transformation zones. *Phys. Rev. Lett.* **126**, 015501 (2021).
34. Wijtmans, S. & Manning, M. L. Disentangling defects and sound modes in disordered solids. *Soft Matter* **13**, 5649–5655 (2017).
35. De Giuli, E. Renormalization of elastic quadrupoles in amorphous solids. *Phys. Rev. E* **101**, 043002 (2020).
36. Shimada, M., Mizuno, H., Wyart, M. & Ikeda, A. Spatial structure of quasilocalized vibrations in nearly jammed amorphous solids. *Phys. Rev. E* **98**, 060901 (2018).
37. Tong, H., Hu, H., Tan, P., Xu, N. & Tanaka, H. Revealing inherent structural characteristics of jammed particulate packings. *Phys. Rev. Lett.* **122**, 215502 (2019).
38. Dederichs, P. H., Lehmann, C., Schober, H. R., Scholz, A. & Zeller, R. Lattice theory of point defects. *J. Nucl. Mater.* **69**, 176–199 (1978).
39. Lerner, E. & Bouchbinder, E. A characteristic energy scale in glasses. *J. Chem. Phys.* **148**, 214502 (2018).
40. Hu, Y.-C. & Tanaka, H. Origin of the boson peak in amorphous solids. *Nat. Phys.* **18**, 669–677 (2022).
41. Brüning, R., St-Onge, D. A., Patterson, S. & Kob, W. Glass transitions in one-, two-, three-, and four-dimensional binary Lennard-Jones systems. *J. Phys. Condens. Matter* **21**, 035117 (2008).
42. Beltukov, Y. M., Fusco, C., Tanguy, A. & Parshin, D. A. Transverse and longitudinal vibrations in amorphous silicon. *J. Phys. Conf. Ser.* **661**, 012056 (2015).
43. Tong, H. & Xu, N. Order parameter for structural heterogeneity in disordered solids. *Phys. Rev. E* **90**, 010401 (2014).
44. Maloney, C. & Lemai^tre, A. Subextensive scaling in the athermal, quasistatic limit of amorphous matter in plastic shear flow. *Phys. Rev. Lett.* **93**, 016001 (2004).
45. Lemai^tre, A. & Maloney, C. Sum rules for the quasi-static and visco-elastic response of disordered solids at zero temperature. *J. Stat. Phys.* **123**, 415–453 (2006).
46. Leonforte, F., Tanguy, A., Wittmer, J. P. & Barrat, J. L. Inhomogeneous elastic response of silica glass. *Phys. Rev. Lett.* **97**, 055501 (2006).
47. Xu, B., Falk, M. L., Patinet, S. & Guan, P. Atomic nonaffinity as a predictor of plasticity in amorphous solids. *Phys. Rev. Mater.* **5**, 025603 (2021).
48. Tung, C.-H. et al. Data-driven insights into the structural essence of plasticity in high-entropy alloys. *JOM* **76**, 5755–5767 (2024).
49. Taraskin, S. N. & Elliott, S. R. Anharmonicity and localization of atomic vibrations in vitreous silica. *Phys. Rev. B* **59**, 8572 (1999).
50. Xu, N., Vitelli, V., Liu, A. J. & Nagel, S. R. Anharmonic and quasi-localized vibrations in jammed solids—Modes for mechanical failure. *Europhys. Lett.* **90**, 56001 (2010).

51. Krisponeit, J.-O. et al. Crossover from random three-dimensional avalanches to correlated nano shear bands in metallic glasses. *Nat. Commun.* **5**, 3616 (2014).
52. Tong, H., Sengupta, S. & Tanaka, H. Emergent solidity of amorphous materials as a consequence of mechanical self-organisation. *Nat. Commun.* **11**, 4863 (2020).
53. Mizuno, H., Shimada, M. & Ikeda, A. Anharmonic properties of vibrational excitations in amorphous solids. *Phys. Rev. Res.* **2**, 013215 (2020).
54. Dong, J. et al. Non-affine atomic rearrangement of glasses through stress-induced structural anisotropy. *Nat. Phys.* **19**, 1896–1903 (2023).
55. Li, H., Xiao, H., Egami, T. & Fan, Y. Infinitely rugged intra-cage potential energy landscape in metallic glasses caused by many-body interaction. *Mater. Today Phys.* **49**, 101582 (2024).
56. Patinet, S., Vandembroucq, D. & Falk, M. L. Connecting local yield stresses with plastic activity in amorphous solids. *Phys. Rev. Lett.* **117**, 045501 (2016).
57. Eshelby, J. D. The determination of the elastic field of an ellipsoidal inclusion, and related problems. *Proc. R. soc. Lond. Ser. A* **241**, 376–396 (1957).
58. Oleg, G., Prabhat, K. J., Itamar, P., Bhaskar Sen, G. & Jacques, Z. Shear transformation zones: state determined or protocol dependent? *Europhys. Lett.* **109**, 16002 (2015).
59. Mungan, M., Sastry, S., Dahmen, K. & Regev, I. Networks and hierarchies: how amorphous materials learn to remember. *Phys. Rev. Lett.* **123**, 178002 (2019).
60. Yip, C.-T. et al. Direct evidence of void-induced structural relaxations in colloidal glass formers. *Phys. Rev. Lett.* **125**, 258001 (2020).
61. Donati, C. et al. Stringlike cooperative motion in a supercooled liquid. *Phys. Rev. Lett.* **80**, 2338 (1998).
62. Pazmiño Betancourt, B. A., Douglas, J. F. & Starr, F. W. String model for the dynamics of glass-forming liquids. *J. Chem. Phys.* **140**, 204509 (2014).
63. Yu, H.-B., Richert, R. & Samwer, K. Structural rearrangements governing Johari-Goldstein relaxations in metallic glasses. *Sci. Adv.* **3**, e1701577 (2017).
64. Dale, J. R., Sartor, J. D., Dennis, R. C. & Corwin, E. I. Hyperuniform jammed sphere packings have anomalous material properties. *Phys. Rev. E* **106**, 024903 (2022).
65. Yanagishima, T., Russo, J., Dullens, R. P. A. & Tanaka, H. Towards glasses with permanent stability. *Phys. Rev. Lett.* **127**, 215501 (2021).
66. Rodney, D. & Schuh, C. Distribution of thermally activated plastic events in a flowing glass. *Phys. Rev. Lett.* **102**, 235503 (2009).
67. Fan, Y., Iwashita, T. & Egami, T. How thermally activated deformation starts in metallic glass. *Nat. Commun.* **5**, 5083 (2014).
68. Hu, Y.-C. & Tanaka, H. Universality of stringlet excitations as the origin of the boson peak of glasses with isotropic interactions. *Phys. Rev. Res.* **5**, 023055 (2023).
69. Gao, L., Yu, H.-B., Schrøder, T. B. & Dyre, J. C. Unified percolation scenario for the α and β processes in simple glass formers. *Nat. Phys.* **21**, 471–479 (2025).
70. Kapteijns, G., Bouchbinder, E. & Lerner, E. Universal nonphononic density of states in 2d, 3d, and 4d glasses. *Phys. Rev. Lett.* **121**, 055501 (2018).
71. Hu, Y.-C. & Tian, J. PyMatterSim: a python data analysis library for computer simulations of materials science, physics, chemistry, and beyond. Prepint at arxiv:2411.17970 [cond-mat] (2024).
72. Tanguy, A., Wittmer, J. P., Leonforte, F. & Barrat, J. L. Continuum limit of amorphous elastic bodies: a finite-size study of low-frequency harmonic vibrations. *Phys. Rev. B* **66**, 174205 (2002).
73. Fan, Z. & Ma, E. Predicting orientation-dependent plastic susceptibility from static structure in amorphous solids via deep learning. *Nat. Commun.* **12**, 1506 (2021).

Acknowledgements

We thank the helpful discussion with T. Lei and Prof. Y.-J. Wang. Y.-C.H. thanks the support from the National Natural Science Foundation of China (Grant No. 52471178). H.T. acknowledges the support by the Grant-in-Aid for Specially Promoted Research (JSPS KAKENHI Grant No. JP20H05619) and Scientific Research (A) (JSPS KAKENHI Grant No. JP18H03675) from the Japan Society of the Promotion of Science (JSPS).

Author contributions

H.T. and Y.-C.H. designed the research, analysed the data, and wrote the paper together. Y.-C.H. performed simulations.

Competing interests

The authors declare no competing interests.

Additional information

Supplementary information The online version contains supplementary material available at https://doi.org/10.1038/s41467-025-60781-7.

Correspondence and requests for materials should be addressed to Yuan-Chao Hu or Hajime Tanaka.

Peer review information *Nature Communications* thanks Daniel Şopu, Hai-Bin Yu, and the other, anonymous, reviewer for their contribution to the peer review of this work. A peer review file is available.